Talanta 207 (2020) 120300

Contents lists available at ScienceDirect

Talanta

journal homepage: www.elsevier.com/locate/talanta

A "signal-on" chemiluminescence biosensor for thrombin detection based on DNA functionalized magnetic sodium alginate hydrogel and metalloporphyrinic metal-organic framework nanosheets

Yanna Lin, Yuanling Sun, Yuxue Dai, Weiyan Sun, Xiaodong Zhu, Hao Liu, Rui Han, Dandan Gao, Chuannan Luo*, Xueying Wang**

Key Laboratory of Interfacial Reaction & Sensing Analysis in Universities of Shandong, School of Chemistry and Chemical Engineering, University of Jinan, Jinan 250022, PR China

ARTICLE INFO

Keywords:
Sodium alginate hydrogel
Metalloporphyrinic metal-organic framework nanosheets
Aptamer
Thrombin
Flow injection chemiluminescence

ABSTRACT

A "signal-on" chemiluminescence biosensor was established for detecting thrombin. The thrombin aptamer1-functionalized magnetic sodium alginate (Malg-Apt1) hydrogel was synthesized by physical interaction between sodium alginate and Ca^{2+}, and it was used in the biosensor for separating and enriching thrombin. Ethylenediamine tetraacetic acid (EDTA) was used to chelate with Ca^{2+} to dissolve the hydrogel and release thrombin. A metalloporphyrinic metal-organic framework nanosheet, named as Cu-TCPP(Co) MOFs, was prepared as signal amplification strategy. Cu-TCPP(Co) MOFs/Au-ssDNA (ssDNA: single-strand DNA) was synthesized for controllable further amplification of chemiluminescent signal. The thrombin aptamer2-functionalized magnetic carbon nanotubes (MCNTs-Apt2) were used as a matrix, and Cu-TCPP(Co) MOFs/Au-ssDNA was adsorbed on the MCNTs by the complementary pairing of the partial bases between ssDNA and Apt2. Compared with ssDNA, Apt2 has a stronger interaction with thrombin. Therefore, thrombin can trigger the release of Cu-TCPP(Co) MOFs/Au-ssDNA to achieve signal amplification. Under the optimal conditions, the biosensor could detect thrombin as low as 2.178×10^{-13} mol/L with the range from 8.934×10^{-13} to 5.956×10^{-10} mol/L and exhibited excellent selectively. Moreover, the "signal-on" chemiluminescence biosensor showed potential application for the detection of thrombin in body fluids.

1. Introduction

Chemiluminescence (CL) is a phenomenon of luminescence produced by chemical reactions. Therefore, CL analysis does not require an external light source, avoiding Rayleigh scattering and Raman scattering. The CL method has a higher signal to noise ratio than the fluorescence method. In addition, the CL method is simple and easy to operate, and has been widely used in environmental [1], pharmaceutical [2] and biological [3] analyses. The application of nanomaterials not only further enhances the sensitivity of CL analysis but also increases selectivity. The group of Lin [4] developed a CL assay based on multi-DNAzymes-functionalized Au NPs to detect thrombin sensitively, which proved that the method has great potential for clinical application.

Natural polysaccharides such as chitin, chitosan, cellulose and sodium alginate are inexpensive and readily available, and have good biocompatibility and biodegradability. Hydrogels based on natural polysaccharides have been widely used in biomedical fields. For example, the team of Zhang [5] constructed chitin hydrogel to obtain biocompatible and biodegradable bioplastics by freeze-drying and successfully used for healing of rabbit granulation tissue. The team [6] also prepared PANI/cellulose composite hydrogels and successfully used them for the regeneration of rat sciatic nerve. In addition, alginate hydrogels are also receiving increasing attention. Due to its unique crosslinking with multivalent cations, alginate hydrogels are widely used for the removal of heavy metal ions in sewage [7–10]. The Marks lab [11,12] combined the carbon nanotubes with calcium alginate to prepare the gel beads with a large adsorption capacity, which were successfully used for the adsorption of bisphenol A in waste water. The research team [13,14] also immobilized bioluminescent bacteria with calcium alginate as a substrate and constructed biosensors for monitoring water toxicity, providing effective methods for water quality

* Corresponding author.
** Corresponding author.
E-mail addresses: chm_yfl518@163.com (C. Luo), chm_wangxy@ujn.edu.cn (X. Wang).

https://doi.org/10.1016/j.talanta.2019.120300
Received 30 March 2019; Received in revised form 6 August 2019; Accepted 24 August 2019
Available online 28 August 2019
0039-9140/

analysis and environmental monitoring. Superior biocompatibility and rich functional groups make alginate hydrogels more and more popular in biosensor. Marks et al. prepared Biotin-Alginate [15] and Pyrrole-Alginate [16] conjugates to construct biosensor for the detection of antibiotic, mitomycin C and catechol. The preparation of these conjugates provides the basis for the immobilization of biomolecules. Márquez et al. [17] developed an enzyme amperometric biosensor for whole blood analysis based on electrodeposited calcium alginate hydrogels with satisfactory results. Zhang et al. [18] constructed an ECL biosensor with good biocompatibility for detecting MCF-7 tumor cells. The biosensor used sodium alginate to load glucose oxidase for efficient signal amplification. M. Turemis et al. [19] immobilized algae cells with calcium alginate gel and developed an optical/amperometric biosensor for cell physiology studies. The biosensor showed a reliable response in a short period of time.

The emergence of aptamer provides an efficient and rapid identification research platform for the chemical biology and biomedical communities. The specific recognition between aptamer and target greatly increases the selectivity of the sensor, but the use of aptamer usually requires the aid of nanomaterials. Carbon nanomaterial family has been widely used in various fields such as water treatment [20], solar cells [21], supercapacitors [22] and bioassays [23]. As one of the carbon nanomaterials, carbon nanotubes have been widely used in biosensors due to their large specific surface area, easy activation and functionalization, excellent electrical conductivity and strong mechanical properties. The aptamer and carbon nanotube can be combined by covalent bond or π-π stacking. Hu et al. [24] bound single-stranded DNA to carboxylated multi-walled carbon nanotubes via amide bonds for the construction of electrochemical sensor and detected microRNA sensitively. Zhang et al. [25] constructed a biosensor based on the π-π stacking between aptamers and carbon nanotubes. The biosensor used carbon nanotubes as a signal indicator to achieve selective detection of H37Rv.

Metalloporphyrin is an important class of biomimetic catalyst with simulated peroxidase activity [26,27]. Although metalloporphyrin exhibits good catalytic effect as homogeneous catalyst, it is susceptible to oxidative degradation and irreversible dimerization in solution, which reduces its catalytic activity. Moreover, it is difficult to separate metalloporphyrin from the system after the catalytic reaction. Metal-organic frameworks (MOFs) not only have high porosity and specific surface area, but also have a strong skeletal structure, which makes it easier to functionalize. The synthesis of functional MOFs is one of the effective methods for making the homogeneous catalysts heterogenize [28–30].

Metalloporphyrin was utilized to construct functional MOFs mainly in two ways: (1) metalloporphyrin was used as organic ligands to prepare MOFs; (2) metalloporphyrin was encapsulated into the pores of MOFs. Metalloporphyrin MOFs have attracted extensive attention due to the combination of the microstructure tunability of MOFs and the unique catalytic activity of the imitation enzyme catalyst metalloporphyrin. Kitagawa et al. [31] synthesized a perfectly crystalline MOF thin film by layer-by-layer growth and Langmuir-Blodgett methods at room temperature. The film was composed of 5,10,15,20-tetrakis(4-carboxyphenyl)porphyrinato-cobalt(II) (CoTCPP) and pyridine, with Cu^{2+} as the node. It was named as NASF-1, which means nano-film of metal-organic frameworks on surface NO. 1. Then, they replaced the building unit with H_2TCPP and synthesized H_2TCPP-Cu (NASF-2) in the same way [32]. The group of Zhang [33] grew Au NPs on Cu-TCPP(M) two-dimensional nanosheets, in which Au NPs possess GOx-like activity and Cu-TCPP has peroxidase activity. Due to the GOx-like and peroxidase activity of the Au NPs/Cu-TCPP(M) hybrid nanosheets, it was successfully used for colorimetric detection of glucose.

Thrombin is a potent vasoconstrictor and mitogen, a major cause of vasospasm after subarachnoid hemorrhage [34]. Thrombin is also a key factor in vascular pathophysiology [35]. Blood from a ruptured cerebral aneurysm condenses around the cerebral arteries, releasing thrombin, which can cause acute and long-term narrowing of blood vessels. This phenomenon may lead to cerebral ischemia and thrombosis. In addition to its pivotal role in the dynamic process of thrombosis, thrombin also has obvious proinflammatory properties, which may affect the occurrence and development of atherosclerosis [36]. Therefore, the monitoring of thrombin levels in body fluids is particularly important. The detection methods of thrombin mainly include electrochemistry [37–39], fluorescence [40,41], colorimetry [42,43] and CL [44].

Herein, a chemiluminescent biosensor for selective and sensitive detection of thrombin was constructed. The biosensor used the Malg-Apt1 as a separation material to separate and enrich thrombin in a complex system. Next, metalloporphyrinic metal-organic framework nanosheet (named as Cu-TCPP(Co) MOFs), MCNTs-Apt2 and ssDNA-modified Au NPs (Au-ssDNA) were synthesized. Among them, the base of ssDNA was partially complementary to that of the Apt2. Compared with bulk MOFs, sheet-like MOFs could expose more active sites and exert superior catalytic effects. Cu-TCPP(Co) MOFs/Au-ssDNA composites were synthesized by electrostatic interaction between Au NPs and Cu-TCPP(Co) MOFs. The composites aggregate the high catalytic activity of Cu-TCPP(Co) MOFs and Au NPs, which synergistically enhance the catalytic activity. Cu-TCPP(Co) MOFs/Au-ssDNA was immobilized on MCNTs-Apt2 by the principle of base complementary pairing. The binding between Apt2 and thrombin was greater than the binding between Apt2 and ssDNA. When thrombin was present, the composites were released, catalyzing the CL reaction of luminol CL system to construct a “signal-on” CL biosensor and detect thrombin sensitively and selectively.

2. Experimental section

2.1. Reagents and materials

Sodium alginate, $FeCl_3$ and $FeCl_2$ were obtained from Tianjin Damao Chemical Reagent Factory. Nano-Fe_3O_4, $CaCl_2$ and ethylenediaminetetraacetic acid (EDTA) were purchased from Sinopharm Group Reagent Co., Ltd. (Shanghai, China). 1-(3-dimethylaminopropyl)-3-ethylcarbodiimide hydrochloride (EDC, 95%) was bought from Saan Chemical Technology Co., Ltd. (Shanghai, China). *N*-Hydroxysuccinimide (NHS) was supplied by Shanghai Civi Chemical Technology Co., Ltd. (Shanghai, China). $HAuCl_4$ was obtained from Macklin Biochemical Technology Co., Ltd. (Shanghai, China). $Cu(NO_3)_2{\cdot}3H_2O$ was purchased from Tianjin Donghe Chemical Co., Ltd. (Tianjin, China). 5, 10, 15, 20-tetrakis (4-carboxyphenyl) porphyrinato-cobalt(II) was ordered from TCI (Shanghai) Development Co., Ltd. (Shanghai, China). Carbon nanotube was obtained from Deke Island Gold Technology Co., Ltd. (Beijing, China). Apt1, Apt2 and ssDNA were purchased from Sangon Biotechnology Co. Ltd. (Shanghai, China). The nucleic acid sequences of DNA are as follows:

Apt 1: 5′–NH_2–$(CH_2)_6$-ATAGGTTGGTGTGGTTGG-3′;
Apt 2: 5′–NH_2–$(CH_2)_6$-AGTCCGTGGTAGGGCAGGTTGGGGTGACT-3′;
ssDNA: 5′–SH–$(CH_2)_6$-TTTCCCCACTGA-3′;

2.2. Apparatus

JEM-2100 scanning electron microscope (SEM) was employed to obtain the SEM images of MCNTs and Cu-TCPP(Co) MOFs. JEOL1400 transmission electron microscope (TEM) was utilized to record the TEM images of Au NPs and Cu-TCPP(Co) MOFs/Au-ssDNA. Fourier transform infrared spectrum (FTIR) was measured by VERTEX70 Fourier infrared spectrometer. X-ray diffraction (XRD) patterns was carried out with a D8 focus diffractometer (Bruker AXS, Germany). Brunner-Emmet-Teller (BET) measurement of Cu-TCPP(Co) MOFs was acquired on fully automatic surface area and porosity analyzer. All CL experiments were performed on a MPI-F flow injection CL detector (Xi'an Remex Analyse instrument Co., Ltd., China).

2.3. Synthesis of Malg-Apt1

The preparation of magnetic sodium alginate hydrogel was performed according to previous methods with some modifications [45]. Firstly, 1.0 g of sodium alginate powder was dissolved in 100 mL of water to obtain a uniformly dispersed sodium alginate sol. Then, 20 mL of 12.5 mg/mL Fe_3O_4 nanoparticles suspension was added to the above sodium alginate sol, and the magnetic alginate sol was uniformly dispersed after ultrasonication at 25 °C for 30 min. The prepared magnetic sodium alginate sol was transferred in a 10 mL centrifuge tube, and 0.4 mL of 0.1 mol/L $CaCl_2$ was added to the solution under ultrasonic conditions. Unbound Ca^{2+} was removed, and then 1.00 mL of magnetic sodium alginate sol was accurately added to the above centrifuge tube. Subsequently, 0.4 mL of $CaCl_2$ was added dropwise under ultrasonic. Magnetic sodium alginate hydrogel was obtained after incubation for 10 min.

Malg-Apt1 were synthesized according to the previous literature with some modification [46]. 1.0 g sodium alginate was dissolved in 100 mL of water, and EDC/NHS (0.48 g/1.32 g) were added into the solution. After reacting at room temperature for 30 min, 100 μL of 0.56 μmol/L Apt1 was added and incubated for 4 h. The hatched solution was mixed with the above magnetic sodium alginate and incubated for 10 min to obtain Malg-Apt1.

2.4. Preparation of Cu-TCPP(Co) MOFs/Au-ssDNA composites

Firstly, Au NPs was prepared. Under vigorous stirring, 1.2 mL of icy $NaBH_4$ (0.1 mol/L) was added to the mixture of trisodium citrate (0.25 mmol/L) and $HAuCl_4$ (0.25 mmol/L). After aging for 6 h, obtaining a seed solution of Au NPs.

14.4 mL of polyvinylpyrrolidone (M = 10000, 5 wt%), 7.2 mL of ascorbic acid (0.1 mol/L), 5.4 mL of KI (0.2 mol/L) and 1.8 mL $HAuCl_4$ (0.25 mol/L) were added to 72 mL of water, obtaining the growth solution. Then, the prepared seed solution was added to the growth solution. After magnetic stirring for 10 min, Au NPs were washed several times with water and dispersed in 25 mL of water (The concentration of Au NPs was 23.2 mg/mL). 1 mL of 0.95 μmol/L ssDNA was added to 1 mL of Au NPs. After reacting for 0.5 h at room temperature, Au-ssDNA was obtained.

Cu-TCPP(Co) MOFs was prepared referring to the previous literature with some modification [47]. 50 mg $Cu(NO_3)_2{\cdot}3H_2O$ was immersed in the mixture of NaOH (2 mol/L) and ammonium persulfate (0.5 mol/L) for 60 min at 15 °C. Then, $Cu(OH)_2$ suspension was obtained. 50 mg of 5, 10, 15, 20-tetrakis (4-carboxyphenyl) porphyrinato-cobalt(II) was dispersed in 10 mL DMF, and then the above $Cu(OH)_2$ suspension was poured into the porphyrin solution. After fully stirring, the mixture was transferred to a 25 mL autoclave and reacted at 120 °C for 8 h. The supernatant was discarded to give a dark purple sample. The product was rinsed several times with ethanol and deionized water.

100 mg of Cu-TCPP(Co) MOFs was dispersed in 100 mL of PBS, and 0.1 mL of Au-ssDNA was added to the solution. After 20 min, the product was isolated by centrifugation to obtain the Cu-TCPP(Co) MOFs/Au-ssDNA. The precipitate was dispersed in 100 mL of PBS and stored at 4 °C.

2.5. Synthesis of MCNTs-Apt2

2.0 g of CNTs was dispersed in 200 mL mixed acid solution (V_{HNO3}: V_{H2SO4} = 2:1) and sonicate the mixture for 1 h. After being uniformly dispersed, the mixed solution was stirred at 120 °C and refluxed for 1 h. The product was cooled at room temperature and washed to neutrality with abundant water. After vacuum drying, the resulting black sample was carboxylated CNTs.

The synthesis process of MCNTs is as follows: 1.0 g of carboxylated CNTs was dispersed in 200 mL mixed aqueous solution of $FeCl_3$ and $FeCl_2$. Under the protection of N_2, the value of pH was adjusted to 12. Next, the mixture was refluxed at 50 °C for 30 min. The precipitates were isolated in the magnetic field and washed with water and ethanol.

0.2 g of MCNTs was dispersed in PBS (pH 7.4), and then EDC/NHS (0.48 g/1.32 g) were added into the MCNTs suspension. After 30 min, Apt2 was added to the solution and incubated for 4 h at room temperature. Under an external magnetic field, the product was washed with PBS to remove unreacted Apt2 and transferred to a 100 mL volumetric flask for storage at 4 °C.

2.6. Adsorption performance of MCNTs-Apt2

The adsorption properties of MCNTs-Apt2 on Cu-TCPP(Co) MOFs/Au-ssDNA were studied in this work. 1 mg of MCNTs-Apt2 was placed into 25 mL tubes. Next, different volume dose of 1 mg/mL of Cu-TCPP (Co) MOFs/Au-ssDNA were separately added to the multiple tubes. The tubes were shaken at room temperature for 1 h. Under the action of magnetic field, the supernatant of the tubes were detected by a CL analyzer and the adsorption capacities (Q) were calculated.

1 mg of MCNTs-Apt2 was dispersed in 3 mL Cu-TCPP(Co) MOFs/Au-ssDNA, and shaken for 0.5 min, 1min, 3min, 5min, 10 min, 15 min, 20 min and 25 min, respectively. Under the action of magnetic field, the supernatants of different shaking time were detected by a CL analyzer and the adsorption time of MCNTs-Apt2 to Cu-TCPP(Co) MOFs/Au-ssDNA was obtained.

The adsorption capacities were calculated from the following formula:

$$Q = \frac{(c_0 - c_e)V}{m}$$

where Q (mg/mg) was the mass of Cu-TCPP(Co) MOFs/Au-ssDNA adsorbed by unit mass of MCNTs-Apt2, c_0 (mg/mL) and c_e (mg/mL) were the concentration of Cu-TCPP(Co) MOFs/Au-ssDNA in the initial and final solution, respectively. V (mL) was the volume of the adsorption mixture, and m (mg) was the mass of the MCNTs-Apt2.

3. Results and discussion

3.1. Concept of the design

In this work, a sensitive, rapid and specific CL biosensor based on the peroxidase catalytic activity of Cu-TCPP(Co) MOFs/Au-ssDNA is reported. Malg-Apt1 with excellent biocompatibility was used to separate and enrich thrombin from body fluids. The structural similarity of metalloporphyrins to coenzymes found in many enzyme/protein families allows them to be used as artificial enzymes. Combined with the ordered pore structure, large specific surface area and functions of MOFs, Cu-TCPP(Co) MOFs was synthesized. In order to controllably further amplify chemiluminescent signal, Cu-TCPP/Au-ssDNA was synthesized to synergistically catalyze the luminol CL system.

Since the partial base of Apt2 was complementary to that of ssDNA, Cu-TCPP(Co) MOFs/Au-ssDNA was immobilized by MCNTs under the action of external magnetic field. The binding force between aptamer and target is expressed by the equilibrium dissociation constant (K_d) of target-nucleic acid complex. The K_d values of thrombin aptamers (15 bases and 29 bases) were 100 nmol/L and 0.5 nmol/L, respectively. Therefore, when thrombin was present, Cu-TCPP(Co) MOFs/Au-ssDNA with peroxidase activity was released from MCNTs-Apt2, achieving signal amplification, as shown in Scheme 1. As a proof of the concept, Malg-Apt1, Cu-TCPP(Co) MOFs/Au-ssDNA and MCNTs-Apt2 were used to construct the CL biosensor for thrombin detection.

3.2. Characterization of Malg

The freeze-dried Malg was characterized by SEM, as shown in Fig. 1. The freeze-dried Malg possessed a lamellar structure with Fe_3O_4 adhesion, indicating that the Malg was synthesized successfully.

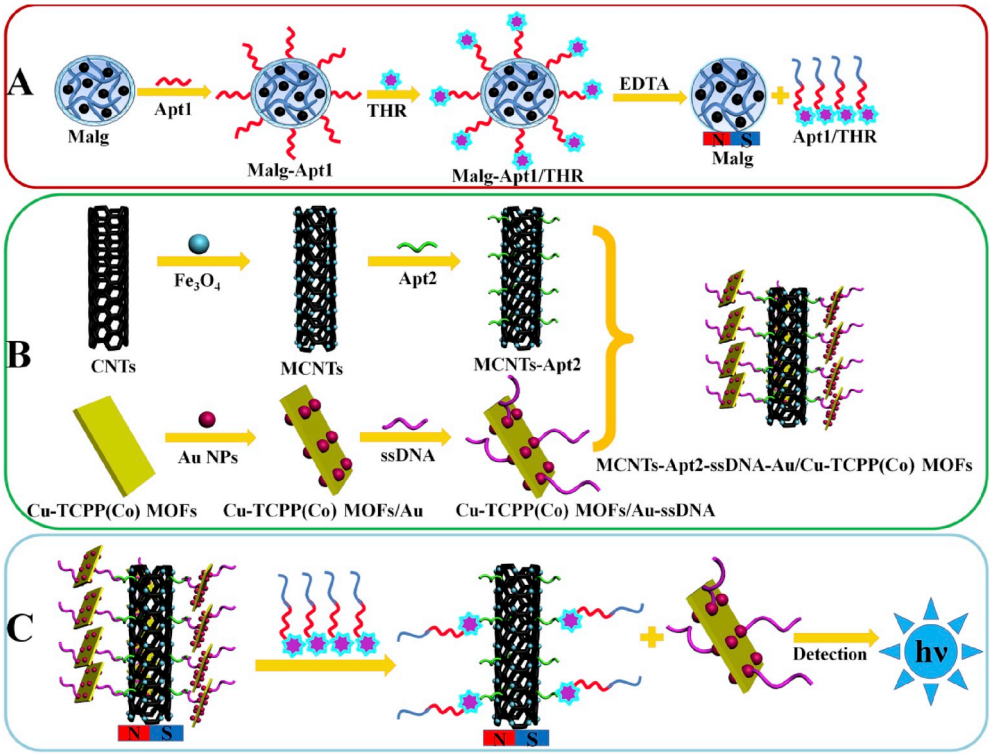

Scheme 1. Schematic illustration of CL sensor.

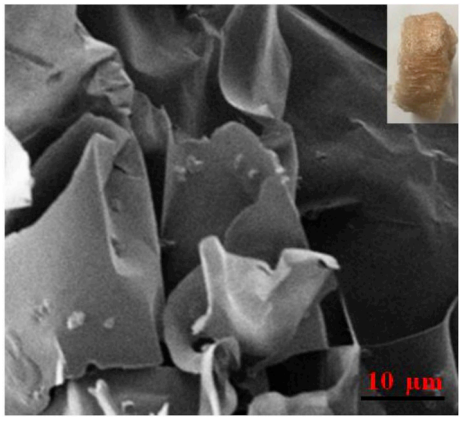

Fig. 1. SEM of Malg.

3.3. Characterization of MCNTs

As the SEM image shows (Fig. 2A), the surface of MCNTs was coated by Fe_3O_4. It can be seen from the XRD patterns (Fig. 2B) that the MCNTs contain six characteristic diffraction peaks (30.2°, 35.5°, 43.2°, 53.6°, 57.1° and 62.7°) of Fe_3O_4, indicating that the Fe_3O_4 was successfully composited on CNTs. As shown in Fig. 2C, the peak at 3445 cm^{-1} is the stretching vibration peak of –OH in the carboxyl group. The peak at 2915 cm^{-1} attributes to the stretching vibration of C–H in aldehyde group. The peaks at 1369 cm^{-1} and 1634 cm^{-1} are the result of skeleton vibration of C=C in aromatic hydrocarbon. 1055 cm^{-1} and 620 $cm^{-1}$are the characteristic peaks of C–O and Fe_3O_4, respectively. SEM, XRD and FTIR show that MCNTs were prepared successfully.

3.4. Characterization of Cu-TCPP(Co) MOFs/Au-ssDNA

TEM was used to elucidate the morphology of Au NPs, Cu-TCPP(Co) MOFs and Cu-TCPP(Co) MOFs/Au-ssDNA. As shown in Fig. 3A, the synthesized Au NPs possess a relatively regular spherical structure with a uniform particle size of about 10 nm. It can be seen from the TEM image (Fig. 3B) that Cu-TCPP(Co) MOFs possess obvious lamellar structure, and the nanosheets expose the material to more catalytic sites, which lays a foundation for catalyzing the luminol CL system. Fig. 3C shows that the Cu-TCPP(Co) MOFs with lamellar structure can adsorb Au NPs by electrostatic interaction and the Au NPs were not agglomeration.

XRD, FTIR and BET were used to explain the crystalline nature of Cu-TCPP(Co) MOFs. As shown in Fig. 4A, the XRD pattern shows the

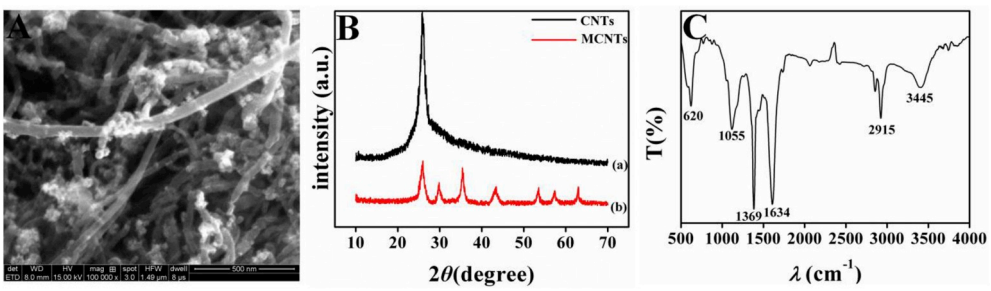

Fig. 2. SEM (A), XRD (B) and FTIR (C) of MCNTs.

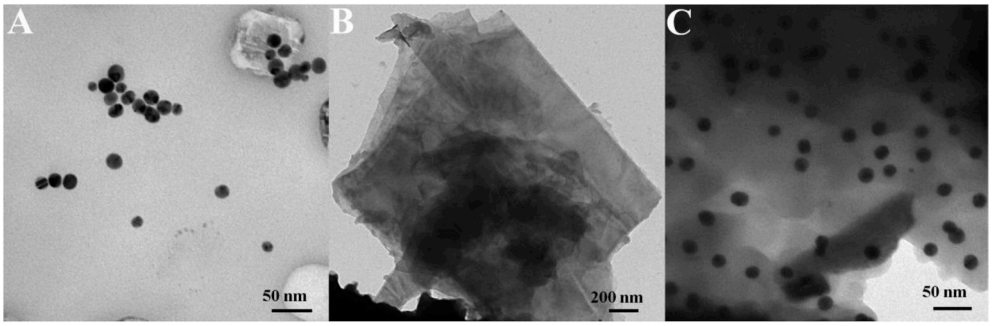

Fig. 3. TEM of Au NPs (A), Cu-TCPP(Co) MOFs (B), Cu-TCPP(Co) MOFs/Au-ssDNA (C).

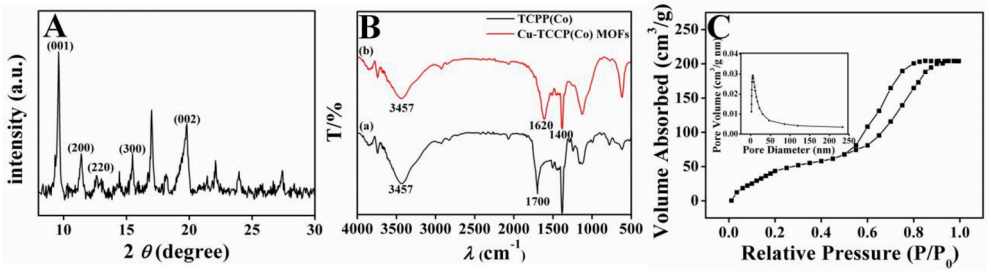

Fig. 4. XRD (A), FTIR (B) and BET (C) of Cu-TCPP(Co) MOFs.

(001), (200), (220), (300), (002) crystal faces of as-prepared Cu-TCPP (Co) MOFs, which is consistent with those reported in the literature [48,49]. In Fig. 4B(a), 3457 cm^{-1} is the –OH stretching vibration in the carboxyl group, and 1700 cm^{-1} is the C–O stretching vibration in the carboxyl group. Interestingly, as shown in Fig. 4B(b), the C–O stretching vibration peak at 1700 cm^{-1} disappears and the stretching vibration absorption peak of Cu–O–Cu appears at 1620 cm^{-1} and 1400 cm^{-1}, indicating that the Cu-TCPP(Co) MOFs was synthesized successfully. The BET properties of Cu-TCPP(Co) MOFs are shown in Fig. 4C. The synthesized Cu-TCPP(Co) MOFs are type IV adsorption isotherms with a mesoporous structure and the pore diameter of about 5.55 nm. What's more, the specific surface area of Cu-TCPP(Co) MOFs was 413.1274 m^2/g.

3.5. CL assay for different systems

The CL behavior of different systems was investigated under alkaline conditions. NaOH-luminol-H_2O_2, NaOH-luminol–H_2O_2–Cu-TCPP (Co) MOFs, NaOH-luminol–H_2O_2–Au NPs, NaOH-luminol–H_2O_2–Cu-TCPP(Co) MOFs/Au CL systems were constructed, and its CL properties are shown in Fig. 5. As shown in Fig. 5a, the CL intensity of NaOH-luminol-H_2O_2 system is weak when no catalyst was present. When Au NPs or Cu-TCPP(Co) MOFs was added to the CL system (Fig. 5b, c), the CL intensity of NaOH-luminol-H_2O_2 system was enhanced. It is worth noting that the CL intensity of NaOH-luminol-H_2O_2 CL system was greatly enhanced in the presence of Cu-TCPP(Co) MOFs/Au-ssDNA (Fig. 5d), indicating that the prepared composites possess significant signal amplification effect on the CL system.

3.6. Peroxidase-like activity of Cu-TCPP(Co) MOFs/Au

It is known from the CL assay that the prepared Cu-TCPP(Co) MOFs/Au composites have a strong catalytic effect on NaOH-luminol-H_2O_2 CL system. To explore its peroxidase-like activity, the Michaelis-Menten constant (K_m) was calculated using the Lineweaver-Burk: $\frac{1}{\nu} = \frac{K_m}{V_{max}}\frac{1}{[S]} + \frac{1}{V_{max}}$, where ν is initial velocity, V_{max} is the maximum velocity, [S] represents the concentration of substrate. The V_{max} and K_m of Cu-TCPP

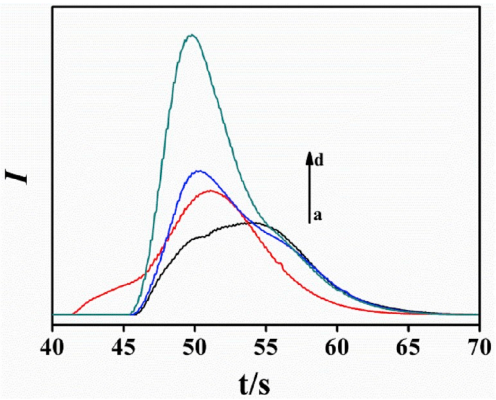

Fig. 5. The CL spectrum of different systems. (a) NaOH-luminol-H_2O_2, (b) NaOH-luminol–H_2O_2–Cu-TCPP(Co) MOFs, (c) NaOH-luminol–H_2O_2–Au NPs, (d) NaOH-luminol–H_2O_2–Cu-TCPP(Co) MOFs/Au-ssDNA.

(Co) MOFs/Au were calculated based on the Lineweaver-Burk. As shown in Fig. 6, the K_m value of Cu-TCPP(Co) MOFs/Au for H_2O_2 was 0.35 mmol/L, which is similar to that of HRP (0.34 mmol/L) [50]. This calculation indicates that Cu-TCPP(Co) MOFs/Au could replace biological enzyme and has similar properties to HRP.

Based on the peroxidase-like activity of Cu-TCPP(Co) MOFs/Au, we speculate that the possible mechanism is as follows:

Firstly, Cu^{2+} and Co^{2+} contained in the Cu-TCPP(Co) MOFs/Au, the transition metal ions can undergo Fenton reaction, thus showing peroxidase-like activity. The reaction process of Cu^{2+} can be expressed as formulas (1–5).

$$H_2O_2 + Cu^{2+} \rightarrow Cu^{3+} + \cdot OH + OH^- \quad (1)$$

$$H_2O_2 + Cu^{3+} + OH^- \rightarrow Cu^{2+} + \cdot OOH + H_2O \quad (2)$$

$$Cu^{3+} + OH^- + \bullet OOH \longrightarrow Cu^{2+} + {}^{\bullet}O_2^- + H_2O \quad (3)$$

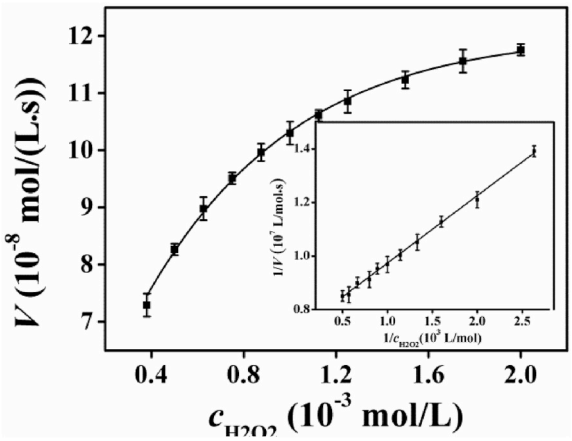

Fig. 6. Steady-state kinetic assays of the Cu-TCPP(Co) MOFs/Au for H_2O_2.

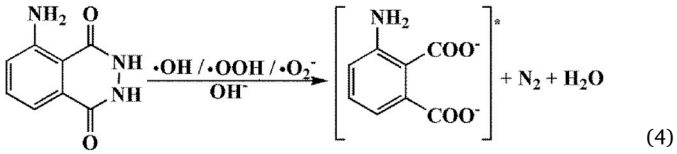
(4)

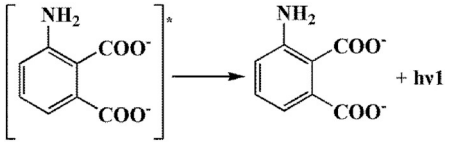
(5)

The reaction process of Co^{2+} is as follows (formula 6-10):

$$H_2O_2 + Co^{2+} \rightarrow Co^{3+} + \cdot OH + OH^- \quad (6)$$

$$H_2O_2 + Co^{3+} + OH^- \rightarrow Co^{2+} + \cdot OOH + H_2O \quad (7)$$

$$Co^{3+} + OH^- + \bullet OOH \longrightarrow Co^{2+} + \bullet O_2^- + H_2O \quad (8)$$

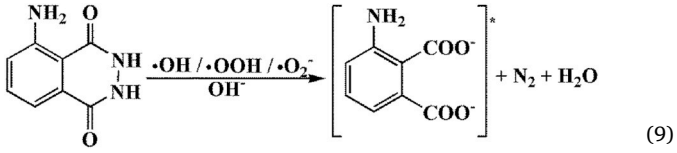
(9)

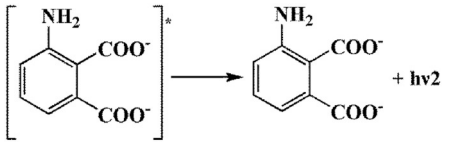
(10)

Under alkaline conditions, the peroxidase-like activity of Au NPs in the presence of H_2O_2 can be demonstrated as follows (formula 11-13):

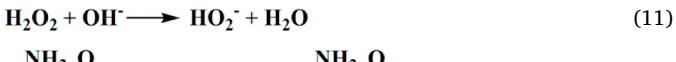
(11)

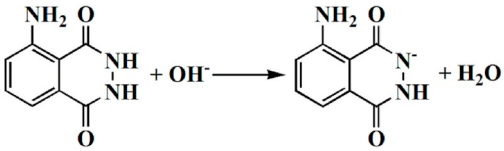
(12)

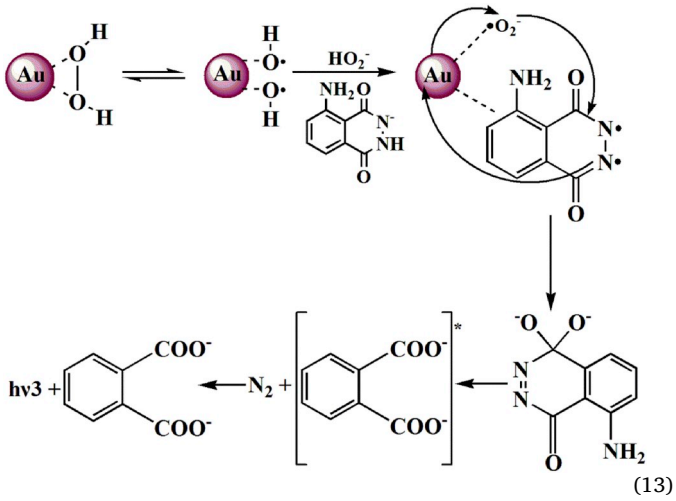
(13)

Porphyrin molecules have large planar conjugated structure and stable macrocyclic rigid structure. There is a strong absorption band around 400 nm, which reduces the difference between the LUMO level and the HOMO level in the porphyrin molecular orbital, and improves the speed and efficiency of electron transfer. It can be inferred that the high peroxidase-like activity of the Cu-TCPP(Co) MOFs/Au may be the result of the interaction of transition ions, Au NPs and porphyrin molecules.

3.7. Adsorption properties of MCNTs-Apt2

As shown in Fig. 7, the adsorption properties of MCNTs-Apt2 on Cu-TCPP(Co) MOFs/Au-ssDNA were explored. The adsorption capacity of Cu-TCPP(Co) MOFs/Au-ssDNA by MCNTs-Apt2 is shown in Fig. 7A, and the adsorption capacity increases as the concentration of Cu-TCPP(Co) MOFs/Au-ssDNA increases until its concentration reaches 0.006 mg/mL. As a result, the adsorption capacity of MCNTs-Apt2 is 0.3 mg/mg. The adsorption kinetics of MCNTs-Apt2 is shown in Fig. 7B. As it can be seen, MCNTs-Apt2 can achieve maximum adsorption of Cu-TCPP(Co) MOFs/Au-ssDNA within 10 min.

3.8. Optimization of CL biosensor conditions

To ensure high sensitivity of the CL biosensor, the conditions of CL

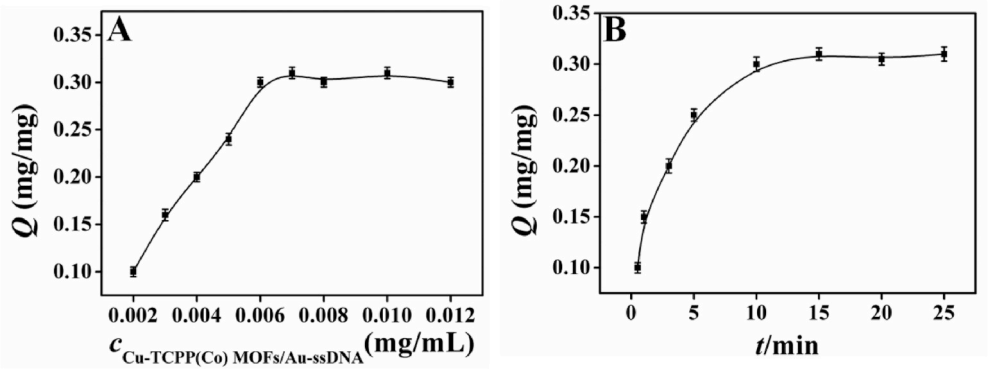

Fig. 7. The adsorption properties of MCNTs-Apt2.

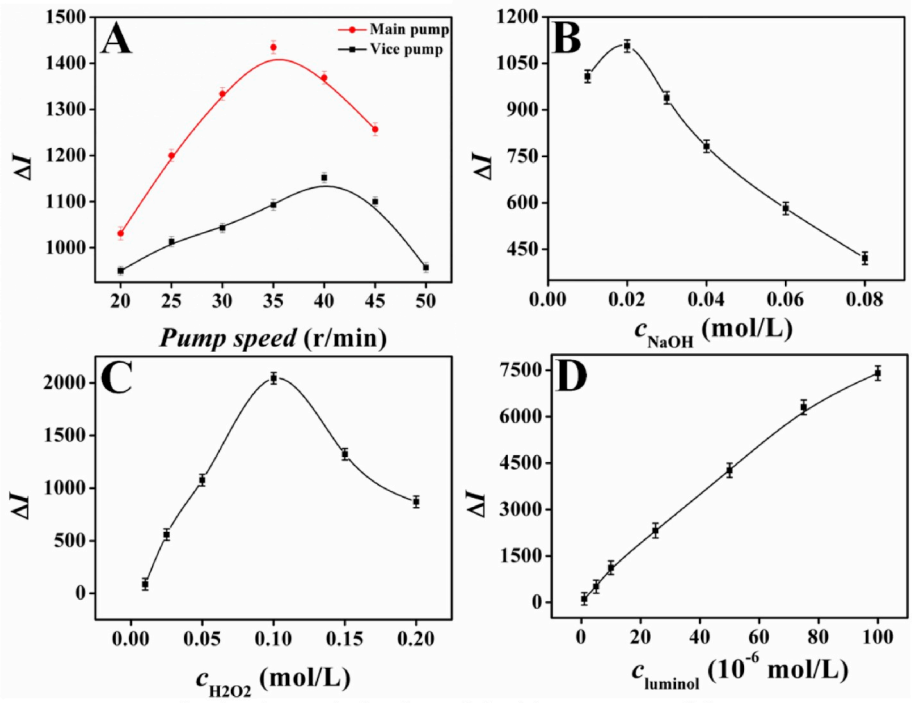

Fig. 8. The optimization of CL biosensor conditions.

biosensor were optimized as shown in Fig. 8.

The pump speed can have an effect on mixedness of solutions, which in turn affects the stability of the biosensor. After optimization, the main pump speed was 35 r/min and the vice pump speed was 40 r/min. NaOH, H_2O_2 and luminol were used to construct the CL system, the concentration of them could affect CL intensity directly. After optimization, the optimum concentration of NaOH and H_2O_2 was 0.02 mol/L, and 0.1 mol/L, respectively. As shown in Fig. 8D, the CL intensity increases with the increasing luminol concentration until it exceeds the instrument range, which may be caused by the catalysis of Cu-TCPP(Co) MOFs/Au. Considering the CL intensity and reagent dosage, 2.5×10^{-5} mol/L was selected as the appropriate concentration of luminol.

3.9. Analytical performance of the CL biosensor

In order to verify the analytical performance of the constructed biosensor, the CL intensity (I_0) of the reference solution and the CL intensity (I) of the system after adding the thrombin standard solution were measured, respectively. Accordingly, the CL intensity difference (ΔI) between I_0 and I was obtained. Fig. 9 shows that as the thrombin concentration increased from 8.9×10^{-13} mol/L to 5.9×10^{-10} mol/L, ΔI increased gradually and a good linear relationship was obtained. The linear correlation equation is $\Delta I = 0.1432c + 1565.2$ (correlation coefficient $R^2 = 0.997$). The detection limit of the method is as low as 2.2×10^{-13} mol/L. The result indicates that the CL biosensor could achieve sensitive detection of thrombin.

CL is one of the methods for detecting thrombin. Some excellent methods for detecting thrombin are shown in Table 1. Compared with those excellent methods, the results show that the CL biosensor constructed in this work also shows superior performance and has a lower detection limit. It can be seen that the Cu-TCPP(Co) MOFs/Au-ssDNA conjugates is an excellent solid mimic peroxidase that can significantly improve the performance of the CL biosensor.

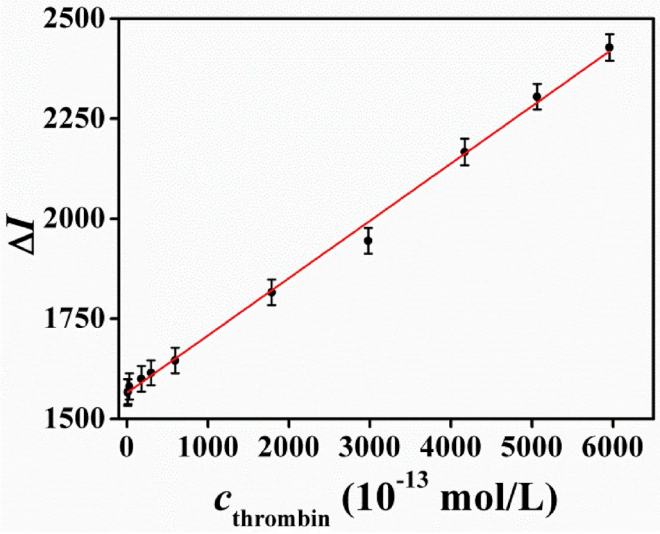

Fig. 9. The standard curve of the CL biosensor.

Table 1
Comparison results of different methods.

Methods	Liner range (mol·L^{-1})	Detection limit (mol·L^{-1})
FL [51]	2.475×10^{-8} – 1.371×10^{-7}	7.5×10^{-9}
CL [4]	1.0×10^{-12} – 2.5×10^{-11}	5.5×10^{-13}
Colorimetry [52]	1.0×10^{-8} – 1.0×10^{-7}	8.3×10^{-9}
FL [53]	2.8×10^{-10} – 8.6×10^{-8}	3.0×10^{-11}
Electrochemistry [54]	1.0×10^{-9} – 5.0×10^{-7}	4.9×10^{-10}
ECL [55]	1.0×10^{-11} – 1.0×10^{-6}	3.5×10^{-12}
This work	8.9×10^{-13} – 5.9×10^{-10}	2.2×10^{-13}

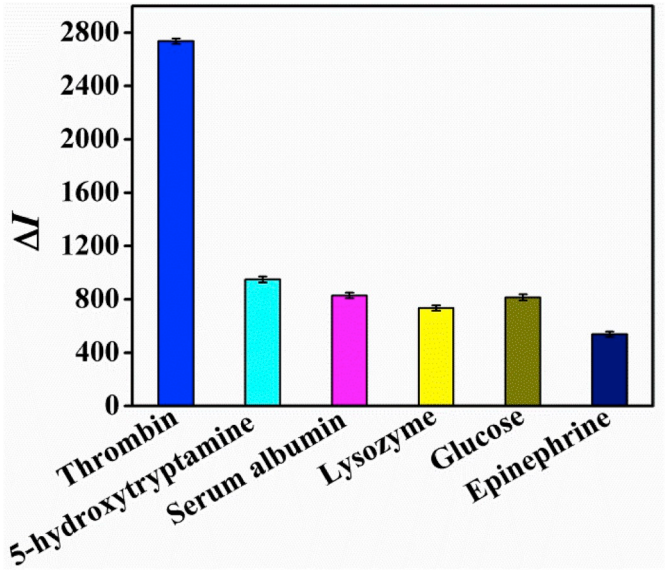

Fig. 10. Selectivity study of CL biosensor.

Table 2
Application of CL sensor.

Samples	Content (10^{-12} nmol/L)	Found (10^{-12} nmol/L)	RSD (%)	Recovery (%)
Serum 1#	46.04	85.69	2.8	99.1
Serum 2#	46.18	86.56	3.1	100.9
Serum 3#	46.02	87.22	2.5	102.9

3.10. Selectivity of the CL biosensor

The selectivity of the biosensor toward thrombin was investigated by recording changes in CL intensity with the addition of 5-hydroxytryptamine, serum albumin, lysozyme, glucose and epinephrine. As indicated in Fig. 10, the biosensor showed a negligible response to the coexistence when compared to its response to thrombin. In addition, c_x was used to represent the concentration at which the coexistence begins to affect the change in the chemiluminescence signal of the CL system, and c was used to indicate the concentration of thrombin in the system. The ratio of c_x to c was called the interference multiplier. Taking into account the influence of the saturation effect, the interference multiplier of the CL biosensor was measured. As shown in Fig. S1, for standard CL assay, the interference multipliers for 5-hydroxytryptamine, serum albumin, lysozyme, glucose and epinephrine were 180, 400, 380, 450 and 200, respectively. For the CL biosensor, the interference multipliers for 5-hydroxytryptamine, serum albumin, lysozyme, glucose and epinephrine were 600, 750, 780, 800 and 680, respectively. The above experimental results demonstrated that the constructed CL biosensor has strong anti-interference ability and good selectivity.

4. Application of the CL biosensor

To verify the feasibility of the constructed CL biosensor in practical applications, the CL biosensor was further applied to the detection of thrombin in serum sample. As shown in Table 2, the recoveries ranged from 99.1% to 102.9% under optimal conditions. All the above results indicate that the constructed CL biosensor could realize the selective and sensitive detection of thrombin in complex biological samples, and possesses the potential for practical application.

5. Conclusion

In summary, Cu-TCPP(Co) MOFs/Au-ssDNA conjugates were first used to construct CL biosensor for protein detection. The reported CL biosensor separates and enriches thrombin with a biocompatible Malg-Apt1. Cu-TCPP(Co) MOFs/Au-ssDNA conjugates were applied in the CL biosensor. The Cu-TCPP(Co) MOFs/Au-ssDNA conjugates integrated the advantages of transition metal ions, porphyrin and Au NPs, and successfully realized the signal amplification of NaOH-luminol-H_2O_2 CL system. The MCNTs-Apt2 was used as the matrix, the Cu-TCPP(Co) MOFs/Au-ssDNA composites were adsorbed on the surface of MCNTs-Apt2 based on the principle of complementary base pairing. When thrombin was presented, Cu-TCPP(Co) MOFs/Au-ssDNA conjugates were released to catalyze the CL system, the "signal-on" CL biosensor was successfully constructed. A concentration of 2.178×10^{-13} mol/L of thrombin could be easily detected. The assay provide a new strategy for thrombin quantification.

Acknowledgements

This work was supported by the Shandong Provincial Natural Science Foundation of China, China (No. ZR2016BM01), Horizontal Scientific Research Project of China (No. W15077), National Natural Science Foundation of China, China (No. 21605094), the Youth Science fund of Shandong Academy of Sciences, China (No. 2017QN006) and Shandong Province Natural Science Institute Joint Fund (No. ZR2015YL006).

Appendix A. Supplementary data

Supplementary data to this article can be found online at https://doi.org/10.1016/j.talanta.2019.120300.

References

[1] Anastasia V. Gribas, Ivan Yu Sakharov, Homogeneous chemiluminescent determination of mercury(II) using a peroxidase-mimicking DNAzyme assay, Anal. Lett. 51 (2018) 1280–1290.
[2] N.A. Alarfaj, S.A. Altamimi, M.F. El-Tohamy, A.M. Almahri, Enhanced SIA-chemiluminescence probes for angiotensin II receptor antagonist detection using silver and gold nanoparticles: applications in pharmaceutical formulations, New J. Chem. 42 (2018) 3383–3393.
[3] Xuanxiang Mao, Yuwan Lu, Xiaodan Zhang, Yuming Huang, β-Cyclodextrin functionalization of metal-organic framework MOF-235 with excellent chemiluminescence activity for sensitive glucose biosensing, Talanta 188 (2018) 161–167.
[4] Junming Wang, Sifeng Mao, Hai-Fang Li, Jin-Ming Lin, Multi-DNAzymes-functionalized gold nanoparticles for ultrasensitive chemiluminescence detection of thrombin on microchip, Anal. Chim. Acta 1027 (2018) 76–82.
[5] He Meng, Xiaolan Wang, Zhenggang Wang, Lingyun Chen, Yao Lu, Xinjiang Zhang, Mei Li, Zhongming Liu, Yu Zhang, Hong Xia, Lina Zhang, Biocompatible and biodegradable bioplastics constructed from chitin via a "green" pathway for bone repair, ACS Sustain. Chem. Eng. 5 (2017) 9126–9135.
[6] Dingfeng Xu, Lin Fan, Lingfeng Gao, Yan Xiong, Yanfeng Wang, Qifa Ye, Aixi Yu, Honglian Dai, Yixia Yin, Jie Cai, Lina Zhang, Micro-nanostructured polyaniline assembled in cellulose matrix via interfacial polymerization for applications in nerve regeneration, ACS Appl. Mater. Interfaces 8 (2016) 17090–17097.
[7] Aiza Gay Corpuz, Priyabrata Pal, Fawzi Banat, Mohammad Abu Haija, Enhanced removal of mixed metal ions from aqueous solutions using flotation by colloidal gas aphrons stabilized with sodium alginate, Separ. Purif. Technol. 202 (2018) 103–110.
[8] Feng Yi, Yayan Wang, Yaquan Wang, Xiong-Fei Zhang, Jianfeng Yao, In-situ gelation of sodium alginate supported on melamine sponge for efficient removal of copper ions, J. Colloid Interface Sci. 512 (2018) 7–13.
[9] Xiaofeng Yi, Fuliang Sun, Zhenhua Han, Fuhao Han, Jiarui He, Minrui Ou, Junjie Gu, Xiaoping Xu, Graphene oxide encapsulated polyvinyl alcohol/sodium alginate hydrogel microspheres for Cu (II) and U (VI) removal, Ecotoxicol. Environ. Saf. 158 (2018) 309–318.
[10] Mothe Gopi Kiran, Pakshirajan Kannan, Gopal Das, Heavy metal removal from aqueous solution using sodium alginate immobilized sulfate reducing bacteria: mechanism and process optimization, J. Environ. Manag. 218 (2018) 486–496.
[11] Maria R. Hartono, Ariel Kushmaro, Robert S. Marks, Xiaodong Chen, Calcium-alginate/carbon nanotubes/TiO_2 composite beads for removal of bisphenol A, Water Sci. Technol. 74 (2016) 1585–1593.
[12] Maria R. Hartono, Robert S. Marks, Xiaodong Chen, Ariel Kushmaro, Hybrid multi-walled carbon nanotubes-alginate-polysulfone beads for adsorption of bisphenol-A

from aqueous solution, Desalin. Water Treat. 54 (2015) 1167–1183.
[13] Evgeni Eltzov, Adiel Yehuda, Robert S. Marks, Creation of a new portable biosensor for water toxicity determination, Sens. Actuators B Chem. 221 (2015) 1044–1054.
[14] Tim Axelrod, Evgeni Eltzov, Robert S. Marks, Bioluminescent bioreporter pad biosensor for monitoring water toxicity, Talanta 149 (2016) 290–297.
[15] Boris Polyak, Shimona Geresh, Robert S. Marks, Synthesis and characterization of a biotin-alginate conjugate and its application in a biosensor construction, Biomacromolecules 5 (2004) 389–396.
[16] Khalil Abu-Rabeah, Boris Polyak, Rodica E. Ionescu, Serge Cosnier, Robert S. Marks, Synthesis and characterization of a Pyrrole alginate conjugate and its application in a biosensor construction, Biomacromolecules 6 (2005) 3313–3318.
[17] A. Márquez, C. Jiménez-Jorquera, C. Domínguez, X. Muñoz-Berbel, Electrodepositable alginate membranes for enzymatic sensors: an amperometric glucose biosensor for whole blood analysis, Biosens. Bioelectron. 97 (2017) 136–142.
[18] Ling Zhang, Yangzhong Wang, Qianqian Tian, Yang Liu, Jinghong Li, Multienzyme decorated polysaccharide amplified electrogenerated chemiluminescence biosensor for cytosensing and cell surface carbohydrate profiling, Biosens. Bioelectron. 89 (2017) 1013–1019.
[19] M. Turemisa, G. Rodioa, G. Pezzotti, E. Touloupakisb, U. Johanningmeierc, I. Bertalanc, S. Litescud, G. Rea, M.T. Giardi, A novel optical/electrochemical biosensor for real time measurement of physiological effect of astaxanthin on algal photoprotection, Sens. Actuators B 241 (2017) 993–1001.
[20] Junhong Wang, Qiang Zhang, Xianzhao Shao, Jianqi Ma, Guanghui Tian, Properties of magnetic carbon nanomaterials and application in removal organic dyes, Chemosphere 207 (2018) 377–384.
[21] Li Chen, Weilin Chen, Enbo Wang, Graphene with cobalt oxide and tungsten carbide as a low-cost counter electrode catalyst applied in Pt-free dye-sensitized solar cells, J. Power Sources 380 (2018) 18–25.
[22] Alex Aboagye, Yiyang Liu, James G. Ryan, Jianjun Wei, Lifeng Zhang, Hierarchical carbon composite nanofibrous electrode material for high-performance aqueous supercapacitors, Mater. Chem. Phys. 214 (2018) 557–563.
[23] Yashuang Hei, Xiqian Li, Xiao Zhou, Jingju Liu, Mehboob Hassan, Siyi Zhang, Yu Yang, Xiangjie Bo, Hsing-Lin Wang, Ming Zhou, Cost-effective synthesis of three-dimensional nitrogen-doped nanostructured carbons with hierarchical architectures from the biomass of sea-tangle for the amperometric determination of ascorbic acid, Anal. Chim. Acta 1029 (2018) 15–23.
[24] Fang Hu, Wancun Zhang, Jiaqi Zhang, Qi Zhang, Tao Sheng, Yueqing Gu, An electrochemical biosensor for sensitive detection of microRNAs based on target-recycled non-enzymatic amplification, Sens. Actuators B 271 (2018) 15–23.
[25] XiaoQing Zhang, Feng Ye, QiongQiong Yao, Fengjiao He, Selection of a new mycobacterium tuberculosis H37Rv aptamer and its application in the construction of a SWCNT/aptamer/Au-IDE MSPQC H37Rv sensor, Biosens. Bioelectron. 98 (2017) 261–266.
[26] Hiroyasu Yamaguchi, Kaori Tsubouchi, Kazuhide Kawaguchi, Eri Horita, Akira Harada, Peroxidase activity of cationic metalloporphyrin-antibody complexes, Chem. Eur J. 10 (2004) 6179–6186.
[27] Eui-Jin Kim, Eun-Kyoung Oh, Jeong K. Lee, Peroxidase and photoprotective activities of magnesium protoporphyrin IX, J. Microbiol. Biotechnol. 24 (2014) 36–43.
[28] Yao Chen, Hoang Tran, Shengqian Ma, Biomimetic catalysis of a porous iron-based metal-metalloporphyrin framework, Inorg. Chem. 51 (2012) 12600–12602.
[29] Jiewei Liu, Yan-Zhong Fan, Xin Li, Zhangwen Wei, Yao-Wei Xu, Li Zhang, Cheng-Yong Su, A porous rhodium(III)-porphyrin metal-organic framework as an efficient and selective photocatalyst for CO_2 reduction, Appl. Catal. B Environ. 231 (2018) 173–181.
[30] Fucheng Leng, Hang Liu, Meili Ding, Qi-Pu Lin, Hai-Long Jiang, Boosting photocatalytic hydrogen production of porphyrinic MOFs: the metal location in metalloporphyrin matters, ACS Catal. 8 (2018) 4583–4590.
[31] Rie Makiura, Soichiro Motoyama, Yasushi Umemura, Hiroaki Yamanaka, Osami Sakata, Hiroshi Kitagawa, Surface nano-architecture of a metal-organic framework, Nat. Mater. 9 (2010) 565–571.
[32] Soichiro Motoyama, Rie Makiura, Osami Sakata, Hiroshi Kitagawa, Highly crystalline nanofilm by layering of porphyrin metal organic framework sheets, J. Am. Chem. Soc. 133 (2011) 5640–5643.
[33] Ying Huang, Meiting Zhao, Shikui Han, Zhuangchai Lai, Jian Yang, Chaoliang Tan, Qinglang Ma, Qipeng Lu, Junze Chen, Xiao Zhang, Zhicheng Zhang, Bing Li, Bo Chen, Zong Yun, Hua Zhang, Growth of Au nanoparticles on 2D metalloporphyrinic metal-organic framework nanosheets used as biomimetic catalysts for cascade reactions, Adv. Mater. 29 (2017).
[34] H. Kasuya, T. Shimizu, K. Takakura, Thrombin activity in CSF after SAH is correlated with the degree of SAH, the persistence of subarachnoid clot and the development of vasospasm, Acta Neurochir. 140 (1998) 579–584.
[35] Julian Ilcheff Borissoff, Henri M.H. Spronk, Sylvia Heeneman, Hugo ten Cate, Is thrombin a key player in the 'coagulation-atherogenesis' maze? Cardiovasc. Res. 82 (2009) 392–403.
[36] J.A. Páramo, The hemostatic system as a modulator of atherosclerosis, N. Engl. J. Med. 365 (2011) 278–279.
[37] Yaxing Zhang, Jianfei Xia, Feifei Zhang, Zonghua Wang, Qingyun Liu, Ultrasensitive label-free homogeneous electrochemical aptasensor based on sandwich structure for thrombin detection, Sens. Actuators B 267 (2018) 412–418.
[38] Taotao Fan, Yan Du, Yao Yao, Jing Wu, Si Meng, Jianjun Luo, Xing Zhang, Dongzhi Yang, Chunyan Wang, Yong Qian, Fenglei Gao, Rolling circle amplification triggered poly adenine-gold nanoparticles production for label-free electrochemical detection of thrombin, Sens. Actuators B 266 (2018) 9–18.
[39] Yu-Cheng Zhou, Xiao-Xue Ran, An-Yi Chen, Ya-Qin Chai, Ruo Yuan, Ying Zhuo, Efficient electrochemical self-catalytic platform based on L-cys-hemin/G-quadruplex and its application for bioassay, Anal. Chem. 90 (2018) 9109–9116.
[40] Saurabh Umrao, Vasundhara Jain, Anusha, Banani Chakraborty, Rahul Roy, Protein-induced fluorescence enhancement as aptamer sensing mechanism for thrombin detection, Sens. Actuators B 267 (2018) 294–301.
[41] Dongxiao Wen, Minhui He, Kefeng Ma, Ying Cui, Jinming Kong, Huaixia Yang, Qingyun Liu, Highly sensitive fluorometric determination of thrombin by on-chip signal amplification initiated by terminal deoxynucleotidyl transferase, Microchimica Acta 185 (2018) 380–387.
[42] Li Li, Yu Liang, Yan Zhao, Zhengbo Chen, Target binding and DNA hybridization-induced gold nanoparticle aggregation for colorimetric detection of thrombin, Sens. Actuators B 262 (2018) 733–738.
[43] Mei Liu, Jiao Li, Baoxin Li, A colorimetric aptamer biosensor based on cationic polythiophene derivative as peroxidase mimetics for the ultrasensitive detection of thrombin, Talanta 175 (2017) 224–228.
[44] Yanna Lin, Jianbo Li, YanhuiWang, Yuanling Sun, Chaofan Ding, Weiyan Sun, Chuannan Luo, A chemiluminescence biosensor for the detection of thrombin based on the aptamer composites, Spectrochim. Acta A Mol. Biomol. Spectrosc. 192 (2018) 153–158.
[45] G. Prabha, V. Raj, Sodium alginate–polyvinyl alcohol-bovin serum albumin coated Fe_3O_4 nanoparticles as anticancer drug delivery vehicle: doxorubicin loading and in vitro release study and cytotoxicity to HepG2 and L02 cells, Mater. Sci. Eng. C 79 (2017) 410–422.
[46] Min Xie, Ning-Ning Lu, Shi-Bo Cheng, Xue-Ying Wang, Ming Wang, Shan Guo, Cong-Ying Wen, Jiao Hu, Dai-Wen Pang, Wei-Hua Huang, Engineered decomposable multifunctional nanobioprobes for capture and release of rare cancer cells, Anal. Chem. 86 (2014) 4618–4626.
[47] Duc La Duong, Hoai Phuong Nguyen Thi, Yong Shin Kim, Anushri Rananaware, Sheshanath V. Bhosale, Facile fabrication of Cu(II)-porphyrin MOF thin films from tetrakis(4-carboxyphenyl)porphyrin and $Cu(OH)_2$ nanoneedle array, Appl. Surf. Sci. 424 (2017) 145–150.
[48] R. Makiura, S. Motoyama, Y. Umemura, H. Yamanaka, O. Sakata, H. Kitagawa, Nat. Mater. 9 (2010) 565.
[49] G. Xu, T. Yamada, K. Otsubo, S. Sakaida, H. Kitagawa, J. Am. Chem. Soc. 134 (2012) 16524.
[50] R. Li, Y. Zhou, L. Zou, S. Li, J. Wang, C. Shu, C. Wang, J. Ge, L. Ling, In situ growth of gold nanoparticles on hydrogen-bond supramolecular structures with high peroxidase-like activity at neutral pH and their application to one-pot blood glucose sensing, Sens. Actuators B 245 (2017) 656–664.
[51] Shahrzad Dehghani, Noor Mohammad Danesh, Mohammad Ramezani, Mona Alibolandi, Parirokh Lavaee, Mojgan Nejabat, Khalil Abnous, Seyed Mohammad Taghdisi, A label-free fluorescent aptasensor for detection of kanamycin based on dsDNA-capped mesoporous silica nanoparticles and Rhodamine B, Anal. Chim. Acta 1030 (2018) 142–147.
[52] Yawei Wang, Jingxing Guo, Yuehua Guo, Xiaobo Zhang, Huangxian Ju, Enzymatically driven formation of palindromic DNA-Au nanoparticles for snowball assembly and colorimetric biosensing, Sens. Actuators B 267 (2018) 328–335.
[53] Xiaolan Chen, Tingting Li, Xueqin Tu, Lan Luo, Label-free fluorescent aptasensor for thrombin detection based on exonuclease I assisted target recycling and SYBR Green I aided signal amplification, Sens. Actuators B 265 (2018) 98–103.
[54] Saeromi Chung, Jong-Min Moon, Jaekyu Choi, Hyundoo Hwang, Yoon-Bo Shim, Magnetic force assisted electrochemical sensor for the detection of thrombin with aptamer-antibody sandwich formation, Biosens. Bioelectron. 117 (2018) 480–486.
[55] Lu Tan, Junjun Ge, Jiao Meng, Jie Guifen, Shuyan Niu, Amplified electrochemiluminescence detection of DNA based on novel quantum dots signal probe by multiple cycling amplification strategy, Talanta 183 (2018) 108–113.